***PREPRINT**: Blocken B, Stathopoulos T, Carmeliet J. 2007. CFD simulation of the atmospheric boundary layer:– wall function problems. Atmospheric Environment 41(2): 238-252. © Elsevier 2007.*

CFD simulation of the atmospheric boundary layer: wall function problems

Bert Blocken [a,*] , Ted Stathopoulos [b], Jan Carmeliet [a,c]

(a) Building Physics and Systems, Technische Universiteit Eindhoven, P.O. box 513, 5600 MB Eindhoven, the Netherlands
(b) Department of Building, Civil and Environmental Engineering, Concordia University, 1455 de Maisonneuve Blvd West, H3G 1M8, Montreal, Quebec, Canada
(c) Laboratory of Building Physics, Department of Civil Engineering, Katholieke Universiteit Leuven, Kasteelpark Arenberg 40, 3001 Leuven, Belgium

*** Corresponding author:** B. Blocken, Building Physics and Systems, Technische Universiteit Eindhoven, P.O. box 513, 5600 MB Eindhoven, the Netherlands.
Tel.: +31 (0)40 247 2138, Fax +31 (0)40 243 8595, E-mail: b.j.e.blocken@tue.nl

Abstract

Accurate Computational Fluid Dynamics (CFD) simulations of atmospheric boundary layer (ABL) flow are essential for a wide variety of atmospheric studies including pollutant dispersion and deposition. The accuracy of such simulations can be seriously compromised when wall function roughness modifications based on experimental data for sand grain roughened pipes and channels are applied at the bottom of the computational domain. This type of roughness modification is currently present in many CFD codes including Fluent 6.2 and Ansys CFX 10.0, previously called CFX-5. The problems typically manifest themselves as unintended streamwise gradients in the vertical mean wind speed and turbulence profiles as they travel through the computational domain. These gradients can be held responsible – at least partly – for the discrepancies that are sometimes found between seemingly identical CFD simulations performed with different CFD codes and between CFD simulations and measurements. This paper discusses the problem by focusing on the simulation of a neutrally stratified, fully developed, horizontally homogeneous ABL over uniformly rough, flat terrain. The problem and its negative consequences are discussed and suggestions to improve the CFD simulations are made.

Keywords: Computational Fluid Dynamics (CFD); Numerical simulation; Atmospheric Boundary Layer (ABL); Sustainable boundary layer; Equilibrium vertical profiles; Horizontal homogeneity

1. Introduction

Computational Fluid Dynamics (CFD) is increasingly being used to study a wide variety of processes in the lower parts of the atmospheric boundary layer (ABL) (0 - 200 m) including pollutant dispersion and deposition, wind-driven rain, building ventilation, etc. Recently, comprehensive literature reviews on the use of CFD for these applications have been published (Stathopoulos, 1997; Reichrath and Davies, 2002; Blocken and Carmeliet, 2004; Bitsuamlak et al., 2004; Meroney, 2004; Franke et al., 2004).

Accurate simulation of ABL flow in the computational domain is imperative to obtain accurate and reliable predictions of the related atmospheric processes. In a CFD simulation, the flow profiles of mean wind speed and turbulence quantities that are applied at the inlet plane of the computational domain are generally fully-developed, equilibrium profiles. These profiles should be representative of the roughness characteristics of that part of the upstream terrain that is not included in the computational domain (i.e. the terrain upstream of the inlet plane). This is expressed by the presence of either the appropriate aerodynamic roughness length y_0 or the appropriate power-law exponent α of this terrain in the expressions of the inlet profiles (Davenport, 1960; 1961; Wieringa, 1992). Within the computational domain, generally three different regions can be distinguished, as illustrated in Figure 1: (1) the central region of the domain where the actual obstacles (buildings, trees, stacks, etc.) are modelled explicitly with their geometrical shape; and (2) the upstream and downstream region of the domain where the actual obstacles are modelled implicitly, i.e. their geometry is not included in the domain but their effect on the flow can be modelled in terms of roughness, e.g. by means of wall functions applied to the bottom of the domain. These wall functions replace the actual roughness obstacles but they should have the same overall effect on the flow as these obstacles. This roughness is expressed in terms of the aerodynamic roughness length y_0 or, less often, in terms of the equivalent sand-grain roughness height for the ABL, $k_{S,ABL}$, which is typically quite high (large-scale roughness; e.g. y_0 in the range of 0.03 m to 2 m (Wieringa, 1992), $k_{S,ABL}$ in the

range of 0.9 m to 60 m). Note that in CFD simulations, often the upstream part of the domain and the terrain outside the domain upstream of the inlet plane are assumed to be of the same roughness, implying that it is not the intention to simulate the development of an internal boundary layer starting from the inlet plane. In the centre of the computational domain, where the actual obstacles are modelled explicitly, additional roughness modelling is limited to the surfaces of the obstacles themselves (walls, roofs, etc.) and the surfaces between these obstacles (streets, grass plains, etc.). This is often also done with wall functions. The roughness of these surfaces is most often expressed in terms of the roughness height k_S that is typically quite small (small-scale roughness; e.g. k_S in the range of 0 to 0.1 m).

The simulation of a horizontally homogeneous ABL over uniformly rough terrain is often required in the upstream and the downstream region of the computational domain. The term "horizontally homogeneous" refers to the absence of streamwise gradients in the vertical profiles of the mean wind speed and turbulence quantities, i.e. these profiles are maintained with downstream distance. This flow type occurs when the vertical mean wind speed and turbulence profiles are in equilibrium with the roughness characteristics of the ground surface. Concerning the upstream part of the domain, a distinction is made between inlet flow, approach flow and incident flow (Fig. 1). The "approach flow" profiles are those travelling towards the building models, while the "incident flow" profiles are those obtained in a similar but empty computational domain, at the position where the buildings would be positioned. Horizontal homogeneity implies that the inlet profiles, the approach flow profiles and the incident profiles are the same.

In the past, several authors have reported difficulties in simulating a horizontally homogeneous ABL flow in at least the upstream part of computational domains. Richards and Younis (1990), discussing the work of Mathews (1987), referred to a situation in which the approach flow changed rapidly in the upstream region of the computational domain. A particular observation was the considerable acceleration of the flow near the surface. Zhang (1994), using the k-ε model and the standard wall functions (Launder and Spalding, 1974) without roughness modification, reported an unwanted change in the profiles of mean wind speed and especially turbulent kinetic energy, which he suggested to be responsible for some of the discrepancies found between the CFD simulations and the corresponding wind tunnel measurements. A similar problem for turbulent kinetic energy was reported by Quinn et al. (2001) who used the k-ε model in CFX-4.1. Riddle et al. (2004), employing Fluent 6 with the k-ε and the Reynolds Stress Model (RSM), observed significant profile changes in an empty computational domain, especially for the turbulent kinetic energy. Problems in simulating a horizontally homogeneous ABL flow were also reported by Miles and Westbury (2003), using CFX-5, and by Franke et al. (2004), Franke and Frank (2005) and Blocken and Carmeliet (2006) using Fluent 5 and Fluent 6.

The unintended differences between inlet profiles and incident profiles (i.e., the horizontal homogeneity problem) can be detrimental for the success of CFD simulations given that even minor changes to the incident flow profiles can cause significant changes in the flow field. Indeed, sensitivity studies by Castro and Robins (1977), Miles and Westbury (2003), Gao and Chow (2005) and Blocken et al. (2006) have indicated the important influence of the shape of the vertical incident flow profiles on the simulation results of flow around buildings. Furthermore, the considerable problems in simulating the simple case of a horizontally homogeneous ABL flow suggest that similar or maybe even more serious problems can be expected when more complex cases of ABL flow have to be simulated, e.g. the development of internal boundary layers (IBL) over terrains with roughness changes.

This paper addresses the problem of horizontal homogeneity associated with the use of sand-grain roughness wall functions. This is done by focusing on the CFD simulation of a neutrally stratified, horizontally homogeneous ABL flow over uniformly rough, flat terrain. The reasons for the difficulties possibly encountered are explained, the negative consequences involved are discussed and suggestions to handle them are made. First, in Section 2, the basic requirements for a CFD simulation of ABL flow with sand-grain wall functions are set. Section 3 describes the commonly used, fully-developed ABL inlet profiles for mean wind speed, turbulent kinetic energy and turbulence dissipation rate. In Section 4, the so-called sand-grain roughness wall-function modification is briefly described. Section 5 points to the inconsistency of the basic requirements for ABL flow simulation with these wall functions. In Section 6, the typical negative consequences of this inconsistency are discussed. Section 7 summarizes various remedial measures. Finally, Section 8 concludes the paper.

2. Basic requirements for ABL flow simulation

In almost all CFD simulations of the lower part of the ABL, an accurate description of the flow near the ground surface is required. In such cases, if the wall roughness is expressed by an equivalent sand-grain roughness k_S in the wall functions, four requirements should be simultaneously satisfied. This set of requirements has been distilled from various sources including CFD literature and CFD software manuals (Richards and Hoxey, 1993; Franke et al., 2004; Fluent Inc., 2005; Ansys Ltd., 2005):

(1) A sufficiently high mesh resolution in the vertical direction close to the bottom of the computational domain (e.g. height of first cell < 1 m);

(2) A horizontally homogeneous ABL flow in the upstream and downstream region of the domain;
(3) A distance y_P from the centre point P of the wall-adjacent cell to the wall (bottom of domain) that is larger than the physical roughness height k_S of the terrain ($y_P > k_S$); and
(4) Knowing the relationship between the equivalent sand-grain roughness height k_S and the corresponding aerodynamic roughness length y_0.

The first requirement is important for all computational studies of flow near the surface of the Earth. For instance, for pedestrian wind comfort studies, Franke et al. (2004) state that at least 2 or 3 control volume layers should be provided below pedestrian height (1.75 m). The second requirement implies the insertion of (empirical) information about the ground roughness (roughness of the bottom of the computational domain) into the simulation to prevent streamwise gradients in the flow in the upstream and downstream part of the domain, i.e. outside the main disturbance of the flow field by the explicitly modelled obstacles (Richards and Hoxey, 1993). This generally requires the use of wall functions. The third requirement implies that it is not physically meaningful to have grid cells with centre points within the physical roughness height. This requirement is explicitly mentioned by several commercial CFD codes including Fluent 6.2 (Fluent Inc., 2005) and Ansys CFX 10.0 (Ansys Ltd., 2005). Both codes warn the user to abide by the requirement $y_P > k_S$. In addition, Ansys Ltd. (2005) mentions that violation of this requirement can lead to inaccuracies and to solver failure but it does not elaborate further on this issue. The fourth requirement concerns a relationship that results from matching the ABL mean velocity profile and the wall function in the CFD code and will be discussed later.

All four requirements should be satisfied in the upstream and downstream region of the computational domain, while in the central part, only requirements (1) and (3) must be adhered to. However, it is generally impossible to satisfy all four requirements. This paper focuses on the standard k-ε model by Jones and Launder (1972) used in combination with the standard wall functions by Launder and Spalding (1974). Note however that the validity of the findings and the statements made in the paper is not limited to this type of turbulence model and these wall functions.

3. Fully-developed ABL profiles

For the k-ε model, Richards (1989) proposed vertical profiles for the mean wind speed U, turbulent kinetic energy k and turbulence dissipation rate ε in the ABL that are based on the Harris and Deaves (1981) model. Because the height of the computational domain is often significantly lower than the ABL height, these profiles are generally simplified by assuming a constant shear stress with height (Richards and Hoxey, 1993):

$$U(y) = \frac{u^*_{ABL}}{\kappa} \ln\left(\frac{y + y_0}{y_0}\right) \quad (1)$$

$$k(y) = \frac{u^{*2}_{ABL}}{\sqrt{C_\mu}} \quad (2)$$

$$\varepsilon(y) = \frac{u^{*3}_{ABL}}{\kappa\,(y + y_0)} \quad (3)$$

where y is the height co-ordinate, u^*_{ABL} the ABL friction velocity, κ the von Karman constant (≈ 0.40-0.42) and C_μ a model constant of the standard k-ε model. It can be easily shown that Eqs. (1-3) are an analytical solution to the standard k-ε model if the model constants $C_{\varepsilon 1}$, $C_{\varepsilon 2}$, σ_ε, C_μ are chosen in such a way that Eq. (4) is satisfied (Richards and Hoxey, 1993):

$$\kappa^2 = (C_{\varepsilon 2} - C_{\varepsilon 1})\,\sigma_\varepsilon \sqrt{C_\mu} \quad (4)$$

Similarly, it can be shown that the set of Eq. (2) and Eqs. (5-6) are also an analytical solution to the same model under the same condition (Durbin and Petterson Reif, 2001).

$$U(y) = \frac{u^*_{ABL}}{\kappa} \ln\left(\frac{y}{y_0}\right) \quad (5)$$

$$\varepsilon(y) = \frac{u^{*3}_{ABL}}{\kappa\, y} \quad (6)$$

These profiles are commonly used as inlet profiles for CFD simulations when measured profiles of U and k are not available. It should be noted that these profiles are not only used for simulations with the standard k-ε model but also with other types of turbulence models: RNG k-ε, realizable k-ε, standard k-ω, SST k-ω, the Spalart-

Allmaras model, the Reynolds Stress model, etc. In these cases, the profiles for k and ε are converted into profiles for either the specific dissipation rate ω ($\omega = \varepsilon/C_\mu k$), the turbulent viscosity ratio μ_t/μ or the Reynolds stresses.

4. Standard wall functions with a sand-grain-based roughness modification

Due to the importance of the surface roughness and the high Reynolds numbers associated with ABL flow, the use of wall functions is generally required for near-wall modelling. The wall functions in CFD codes are generally based on the universal near-wall velocity-distribution (law of the wall) that can be modified for the effects of rough surfaces. In this section, the often used roughness modification that is based on experiments with sand-grain roughness is described.

4.1. Law of the wall for fully rough surfaces

The universal law of the wall for a smooth surface is plotted in Figure 2 (dashed line) using the dimensionless variables $u^+ = U/u^*$ and $y^+ = u^*y/\nu$, where U is the mean velocity tangential to the wall, u* is a wall-function friction velocity and ν is the kinematic viscosity. Note that u* can be different from u^*_{ABL}. The near-wall region consists of three main parts: the laminar layer or linear sublayer, the buffer layer and the logarithmic layer. In the linear sublayer, the laminar law holds ($u^+ = y^+$) while in the log layer, the logarithmic law is valid: ($u^+ = \ln(y^+)/\kappa + B$) where the integration constant $B \approx 5.0 - 5.4$ (e.g. Schlichting, 1968; White, 1991). The laminar law is valid below about $y^+ = 5$ and the logarithmic law above about $y^+ = 30$ up to $y^+ = 500$ - 1000. The modification of the log law for rough surfaces is mainly based on the extensive experiments by Nikuradse (1933) for flow in rough, circular pipes that were covered on the inside as tightly as possible with sand grains (sand-grain roughness k_S). The experiments indicated that the mean velocity distribution near rough walls, when plotted in a semi-logarithmic scale, as in Figure 2, has the same slope (1/κ) but a different intercept. The shift of the intercept, ΔB, as shown in Figure 2, is a function of the dimensionless sand-grain roughness height $k_S^+ = u^*k_S/\nu$, also called "dimensionless physical roughness height" or "roughness Reynolds number". The logarithmic law for a rough wall is (Cebeci and Bradshaw, 1977):

$$\frac{U}{u^*} = \frac{1}{\kappa}\ln\left(\frac{u^* y}{\nu}\right) + B - \Delta B(k_s^+) \tag{7}$$

The roughness function ΔB takes different forms depending on the k_S^+ value. Three regimes are distinguished: aerodynamically smooth ($k_S^+ < 2.25$), transitional ($2.25 \le k_S^+ < 90$) and fully rough ($k_S^+ \ge 90$). ABL flow over rough terrain classifies as fully rough because the roughness elements (obstacles) are so large that the laminar sublayer is eliminated and the flow is considered to be independent of the molecular viscosity. Note that this is the case for flow in the upstream and downstream part of the computational domain but not necessarily for the flow over the explicitly modelled surfaces with a small-scale roughness in the central part of the domain. For the fully rough regime, Cebeci and Bradshaw (1977) report the following analytic fit to the sand-grain roughness data of Nikuradse (1933), which was originally provided by Ioselevich and Pilipenko (1974):

$$\Delta B = \frac{1}{\kappa}\ln(k_s^+) - 3.3 \tag{8}$$

Combining Eqs. (7) and (8), with B = 5.2, yields:

$$\frac{U}{u^*} = \frac{1}{\kappa}\ln\left(\frac{u^* y}{\nu k_s^+}\right) + 8.5 \tag{9}$$

This is the logarithmic law of the wall for fully rough surfaces based on sand-grain roughness. Eq. (9) is illustrated in Figure 2 with k_S^+ as a parameter.

4.2. Wall functions for fully rough surfaces

In this paper, the term "sand-grain-roughness wall functions" refers to standard wall functions modified for roughness based on experiments with sand-grain roughness, also called k_S-type wall functions. The k_S-type wall function for mean velocity is obtained by replacing U and y in Eq. (9) by their values in the centre point P of the

wall-adjacent cell: U_P and y_P. Several commercial CFD codes use slightly different k_S-type wall functions than Eq. (9).

4.2.1. Fully rough k_S-type wall function for mean velocity in Fluent 6.2

The wall function in Fluent 6.2 is given by (Fluent Inc., 2005):

$$\frac{U_p u^*}{u_\tau^2} = \frac{1}{\kappa} \ln\left(\frac{E u^* y_p}{\nu(1 + C_s k_s^+)}\right) \tag{10}$$

where the factor $(1 + C_S k_S^+)$ represents the roughness modification, E is the empirical constant for a smooth wall (≈ 9.793) and $u^* = C_\mu^{1/4} k_P^{1/2}$ and $u_\tau = (\tau_w/\rho)^{1/2}$ are two different wall-function friction velocities. k_P is the turbulent kinetic energy in the centre point P, τ_w is the wall shear stress and ρ the fluid density. C_S, the roughness constant, is an attempt to take into account the type of roughness. However due to the lack of specific guidelines, it is generally set at its default value for sand-grain roughened pipes and channels: 0.5. The user inputs in the code are the values k_S and C_S, in Fluent 6.1 and 6.2 with the restriction that C_S should lie in the interval [0;1]. For an equilibrium boundary layer ($u^* = u_\tau$) and when $C_S k_S^+ >> 1$ (fully rough regime with about $C_S > 0.2$), Eq. (10) can be simplified and takes a form similar to Eq. (9):

$$\frac{U_p}{u^*} = \frac{1}{\kappa} \ln\left(\frac{u^* y_P}{\nu C_s k_s^+}\right) + 5.43 \tag{11}$$

4.2.2. Fully rough k_S-type wall function for mean velocity in Ansys CFX 10.0

Ansys CFX 10.0 provides a similar wall function, however with a fixed value for the roughness constant: $C_S = 0.3$ (Ansys Ltd., 2005):

$$\frac{U_p}{u^*} = \frac{1}{\kappa} \ln\left(\frac{u^* y_p}{\nu(1 + 0.3 k_s^+)}\right) + 5.2 \tag{12}$$

In the fully rough regime ($k_S^+ > 90$) it can be rewritten as follows:

$$\frac{U_p}{u^*} = \frac{1}{\kappa} \ln\left(\frac{u^* y_P}{0.3 \nu k_s^+}\right) + 5.2 \tag{13}$$

4.2.3. Wall functions for k and ε

Irrespective of the value of k_S^+, the wall functions for the turbulent quantities are generally given by:

$$k_P = \frac{u^{*2}}{\sqrt{C_\mu}} \tag{14}$$

$$\varepsilon_P = \frac{u^{*3}}{\kappa y_P} \tag{15}$$

Note that in these equations u* carries the effect of the roughness. In Fluent 6, Eq. (14) is not used but instead the k-equation is solved in the wall-adjacent cells.

k_S-type wall functions are not only used for simulations of flow over sand-grain roughened surfaces. Indeed, many CFD codes including Fluent 6.2 and Ansys CFX 10.0 only provide this type of roughness modification. Consequently, CFD simulations over other types of rough surfaces are also made with k_S-type wall functions. In that case, the actual roughness is characterised by an "equivalent" sand-grain roughness height k_S.

5. Inconsistency in the requirements for ABL flow simulation

The fourth requirement for ABL flow simulation mentioned in Section 2 concerns the relationship between k_S and y_0. It provides the equivalent sand-grain roughness height for the ABL, $k_{S,ABL}$. It can be derived by first-order matching (continuity of function and its first derivative) of the ABL velocity profile (Eq. 5) with the wall-function velocity profile in the centre point P of the wall-adjacent cell, as indicated in Figure 3. For Eqs. (9,11,13) a perfect match with Eq. (5) can be obtained, yielding, respectively:

$$k_{S,ABL} = 30\, y_0 \tag{16}$$

$$k_{S,ABL} = \frac{9.793\, y_0}{C_s} \text{ (Fluent)} \tag{17}$$

$$k_{S,ABL} = 29.6\, y_0 \text{ (Ansys CFX)} \tag{18}$$

and $u^*_{ABL} = u^*$ for all three cases. In Eqs. (16-18), the actual value of the constants (30, 9.793 and 29.6) depends to some extent on the value of κ (0.4 – 0.42). In all cases, $k_{S,ABL}$ is clearly much larger than the corresponding aerodynamic roughness length y_0. As an example, for some terrain types in the updated Davenport roughness classification, the following values are obtained: for rough open terrain: $y_0 = 0.1$ m, $k_{S,ABL} \approx 3$ m; for very rough terrain: $y_0 = 0.5$ m, $k_{S,ABL} \approx 15$ m; for city centres: $y_0 = 2$ m, $k_{S,ABL} \approx 60$ m. Cleary, $k_{S,ABL}$ will often be very large in CFD simulations in built environments. Note that a perfect match between Eq. (1) and Eqs. (9,11,13) cannot be achieved since in this case u^*_{ABL} is different from u^*.

To satisfy all four requirements mentioned in Section 2 is generally impossible with the k_S-type wall functions outlined above. The main reason is that the fourth requirement, expressed by Eq. (16), (17) or (18), in combination with the third requirement ($y_P > k_{S,ABL}$) implies that very large (high) control volumes should be used, which is in conflict with the first requirement (high mesh resolution, hence small y_P). Note that in Fluent, the required cell height can be limited to some extent by maximising C_S ($C_S = 1$; see Eq. 17) but that this will often not be satisfactory. The discussion in the remainder of this paper will focus on – but not be limited to – the relationship $k_{S,ABL} \approx 30y_0$. Then, as an example, for a grass-covered plain with a low aerodynamic roughness length $y_0 = 0.03$ m, $k_{S,ABL}$ is about 0.9 m and y_P should be at least equal to this value, yielding cells of minimum 1.8 m height. For larger values of y_0, much larger (higher) cells are needed. It is clear that this requirement conflicts with the need for a high grid resolution near the bottom of the computational domain and that no accurate solutions for near-ground flow can be obtained with cell sizes so large - see also Franke et al. (2004).

6. Discussion

A typical consequence of not adhering to all four ABL flow requirements is the occurrence of unintended streamwise gradients in the vertical profiles of the mean wind speed and turbulence quantities (horizontal inhomogeneity) as the flow travels through the computational domain. The extent of the streamwise gradients depends on the shape of the vertical inlet profiles, the downstream flow distance, the turbulence model, the type of wall function, the grid resolution (y_P), the roughness height (k_S), the roughness constant (C_S) and the boundary conditions at the top and outlet of the domain. A scenario that can explain – at least partly – the problems observed in some previous studies is discussed below. In the scenario the ABL flow profiles at the inlet of the domain are Eqs. (1-3) or Eqs. (2,5-6), which is common practice in CFD simulations of ABL flow.

Given the requirement $y_P > k_S$, the most straightforward choice might be to apply the required high mesh resolution near the bottom of the domain and to insert a k_S-value ($k_{S,ground}$) that is low enough to satisfy $k_{S,ground} < y_P$. Generally, this value will be significantly lower than required for ABL flow simulation ($k_{S,ABL} \approx 30y_0$). E.g. sometimes $k_S = y_0$ has been used. In this case, the change in roughness between the inlet profile that is representative of the terrain upstream of the domain inlet (corresponding to $k_{S,inlet} = k_{S,ABL} \approx 30y_0$) and the actual smaller ground roughness in the upstream part of the computational domain ($k_{S,ground} < 30y_0$) will introduce an Internal Boundary Layer (IBL), in which the wind speed and turbulence profiles will rapidly adapt to the new and smaller roughness, yielding, amongst others, a considerable acceleration of the flow near the surface. This can explain – at least partly – the unintended streamwise gradients observed by several authors mentioned in the introduction.

To illustrate this scenario, CFD simulations of ABL flow were performed in a 2D, empty computational domain with Fluent 6.1.22. Note that a 2D simulation does not truly represent 3D turbulence but that it serves the purpose of illustrating the problem using the standard k-ε model and economically evaluating possible remedial measures. The domain has dimensions L x H = 10 000 m x 500 m. A structured mesh was generated based on grid-sensitivity analysis, with $y_P = 0.25$ m and a total of 46 000 cells, equidistantly spaced in the horizontal direction (cell length $\Delta x = 10$ m). The inlet profiles are taken equal to Eqs. (2,5-6) with $y_0 = 0.1$ m and $u^*_{ABL} = 0.912$ m/s. At the bottom of the domain, the standard wall functions (Eqs. 10,15) in the code are used, with $k_{S,ground} = 0.24$ m (as large as possible while satisfying $k_{S,ground} < y_P$) and with the default roughness constant $C_S =$

0.5. Note that $k_{S,ground} < k_{S,ABL} = 1.959$ m. As also indicated by Richards and Hoxey (1993), specific attention is needed for the boundary condition at the top of the domain. Along the length of this top boundary, the values from the inlet profiles of U, k and ε at this height are imposed (U = 18.5 m/s, k = 2.77 m²/s², ε = 0.0036 m²/s³). This is done by fixing these constant values in the top layer of cells in the domain. The application of this particular type of top boundary condition is important because other top boundary conditions (symmetry, slip wall, etc) can themselves cause streamwise gradients, in addition to those caused by the wall functions. At the outlet, an "outflow" boundary is used, which assumes no streamwise gradients at this location. The 2D Reynolds-Averaged Navier-Stokes (RANS) equations and the continuity equation are solved using the control volume method. Closure is obtained using the standard k-ε model. Pressure-velocity coupling is taken care of by the SIMPLE algorithm. Pressure interpolation is second order. Second-order discretization schemes are used for both the convection terms and the viscous terms of the governing equations. Figure 4 illustrates the simulation results. The figures on the left show the profiles from ground-level up to 500 m height, while the figures on the right only show the lowest 50 m. As the profiles travel downstream, the streamwise gradients become very pronounced, particularly near the ground surface and they exhibit the typical characteristics of a developing IBL. After a considerable distance (about x = 5000 m, not shown in figure) the profiles attain a new equilibrium with the current simulation parameters (i.e., turbulence model, wall functions, values of y_P, k_S, C_S, and top and outlet boundary condition). Note that changes in these parameters will lead to similar observations but to different profiles. Figure 5 illustrates the relative change, i.e. inhomogeneity error e relative to inlet profile, for each of the variables U, k, ε and TI, as a function of downstream distance at two heights (y = 2 m and y = 20 m):

$$e = 100 \cdot \left| \frac{\varphi_{(x)} - \varphi_{(x=0)}}{\varphi_{(x=0)}} \right| \tag{19}$$

where φ represents one of the flow variables. The errors in all variables reach (very) high values with increasing downstream distance. The error curve for ε at y = 2 m shows an overshoot around 100 m. This overshoot is only present near ground-level (below 3 m). It can be attributed to the combined effect of the transition from the inlet profile to a new equilibrium profile, the vertical discretisation of the inlet profiles – to be explained in the next section – and the very steep gradient of the ε-profile near the ground surface. Given the sensitivity of CFD simulation results to the incident flow profiles, the observed gradients can be detrimental for the accuracy of CFD simulations of atmospheric processes in the ABL.

7. Remedial measures and other wall functions

7.1. Remedial measures for k_S-type wall functions with $k_S < y_P$

Various remedial measures to rectify or at least address the errors discussed in the previous section, are presented and discussed here. Some have been suggested previously, others are new. None of them however can be considered totally satisfactory.

(a) Variable height of wall-adjacent cells. Franke et al. (2004) have mentioned abandoning the usual approach of using a constant vertical height of all the cells adjacent to the bottom of the computational domain (first layer of cells near the ground surface). Instead different initial vertical cell heights can be used in different areas of the domain to satisfy Eqs. (16), (17) or (18) at every position in the domain. This implies using higher cells in the upstream and downstream regions (large-scale roughness; $k_{S,ABL} \approx 30y_0$) and lower cells in the central region of the domain (small-scale roughness, small k_S); e.g. Figure 6. The construction of such meshes is a feasible option when the approach flow corresponds to smooth terrain (e.g. rural area, $y_0 = 0.03$ m). For rough terrain however (e.g. urban, $y_0 = 1$ m), Franke et al. (2004) correctly state that reduction of the cell height from 60 m upstream of the model (needed for an inlet flow with $y_0 = 1$ m) to generally less than 0.5 m close to the building model is not evident, even for unstructured meshes. Nevertheless, with this option, a good horizontal homogeneity can be obtained. An additional drawback however is the coarse near-wall mesh distribution at the inlet. This is important because it determines how the analytical, continuous inlet profiles imposed at the inlet are discretised for input into the simulation. This discretisation occurs because each cell only contains one value of each flow variable (in a cell-centred scheme). In case of high near-wall cells, the continuous inlet profiles will be converted into rough discrete profiles. Figure 7 illustrates this problem. Figures 7a and 7b display two near-wall mesh distributions for the simulation case outlined in Section 6 with $y_0 = 0.1$ m and $k_{S,ABL} = 1.959$ m (Eq. 17 with $C_S = 0.5$). The fine near-wall mesh distribution (with $y_P = 0.25$ m) is the one used in the previous simulation. The coarse near-wall mesh distribution (with $y_P = 2$ m) satisfies the requirement $y_P > k_{S,ABL}$, by having wall-adjacent cells with a height of 4 m. Figure 7c and d show the analytical inlet profiles together with the corresponding discrete profiles of U and TI, all at the domain inlet. The discrepancies that are introduced in case of the coarse

mesh, especially near ground level, are very large (up to 100% and more), and motivate the use of a fine near-ground mesh along the entire length of the computational domain.

(b) Explicit modelling of roughness elements. Another option is to explicitly model the upstream and downstream roughness in the computational domain as rectangular blocks in an attempt to fully reproduce the actual roughness effects on the flow. In this case, sand-grain roughness wall functions can be used to model the small-scale roughness of the surfaces of these blocks. This possibility has been pursued by Miles and Westbury (2003) and to some extent by Moonen et al. (2006). Although this is an interesting option, its practical use can be hindered by the time-consuming iterative study needed to obtain the correct configuration of roughness blocks for a certain set of ABL profiles, which is required if this configuration is not known from previous wind tunnel tests. Additional drawbacks are the increased number of cells and the subsequent increase in required computing power and time.

(c) Minimization of upstream domain length. Reducing as much as possible the upstream length of the computational domain will limit the development of streamwise gradients (Blocken et al., 2006), as indicated in Figures 4 and 5. Nevertheless the minimum upstream length, which is the extent of the upstream disturbance of the flow, should always be provided. This option can be useful in those studies where the upstream flow characteristics are of importance rather than the downstream characteristics (e.g. wind-driven rain impact on the windward facades of isolated buildings) but may be insufficient for other cases.

(d) Generation of ABL profiles based on the k_S-type wall functions. Instead of using the ABL inlet profiles mentioned in Section 3, artificial ABL inlet profiles can be generated by first performing a simulation in an empty computational domain with identical parameters (grid, roughness, etc.) as the intended simulation, with the required high mesh resolution and with $k_{S,ground} < y_P$. This simulation can be performed either by using periodic boundary conditions at the inlet and outlet of a short domain or with a very long domain (typically L > 10 000 m). The resulting profiles at the outlet of the domain are the equilibrium profiles of mean wind speed and turbulence quantities that will yield horizontal homogeneity when applied at the inlet of a similar domain. By this calculation, these profiles are actually adjusted to fit the wall functions. An example are the profiles obtained at x = 10 000 m in Figure 4. While this may be a good solution in some cases (Blocken et al. 2004), changing the ABL inlet profiles is not the most straightforward option and should be performed with great care. The obtained profiles should still be realistic and representative for the situation to be simulated but they can be quite different from the traditional equilibrium profiles as obtained by e.g. measurements.

(e) Artificial reduction of turbulent kinetic energy. In case the upstream mean velocity field is of main importance, rather than the upstream turbulence quantities and the downstream flow, a suitable option might be to artificially lower the turbulent kinetic energy at the inlet to decrease the momentum transfer between the fluid layers which in turn decreases the acceleration of the wind speed near the surface (Blocken and Carmeliet, 2006). Application of this option for the simulation case outlined above shows that quite a good horizontal homogeneity of U can be obtained, at least up to x = 500 m (see Fig. 8, where ALK stands for "artificially lower k"). Reduction of k by a factor of 4 was needed to achieve this level of homogeneity for U. The use of this option, in combination with option (c), has been successfully validated for the wind speed conditions upstream of single buildings and has proven to be valuable for CFD simulations of wind-driven rain deposition on the windward facade of isolated buildings where the upstream flow is of main importance (Blocken and Carmeliet, 2002; 2004; 2006). Clearly however, because of the change of inlet turbulent kinetic energy, erroneous predictions will be obtained downstream of the windward building face and for turbulence properties in general.

(f) Wall shear stress boundary condition. A final option to attempt horizontally homogeneous ABL flow simulation is to explicitly specify the wall shear stress $\tau_w = \rho(u^*_{ABL})^2$ associated with the ABL profiles at the bottom of the upstream and downstream region in the domain. This forces the ABL friction velocity (u^*_{ABL}) to be equal to the wall-function friction velocity (u^* and/or u_τ). The result is a very good horizontal homogeneity for both the mean wind speed and turbulence profiles when Eqs. (1-3) or Eqs. (2,5-6) are used. Figure 8 shows that the errors are very small and remain below 5% for the entire length of the domain. Figure 9 compares the inlet profiles and the downstream profiles at x = 10 000 m without corrections and with wall shear stress imposed. The latter option clearly provides a very good horizontal homogeneity. Note however that this boundary condition should only be used in the region outside the disturbance by the building models and that therefore the effect might not be sufficient.

7.2. The ($y_P > k_S$)-requirement and other wall functions

Another possibility to deal with this problem is the use of wall functions for which not all four requirements mentioned in Section 2 need to be satisfied. Several commercial CFD codes including Fluent 6.2 and Ansys CFX 10.0 at present only provide k_S-type wall functions for which these requirements have to be satisfied. However, the $y_P > k_S$ requirement might need to be reconsidered. At present, it is indeed not possible to perform calculations with codes such as Fluent 6.2 or Ansys CFX 10.0 with $k_S > y_P$. As stated previously, this seems logical because it is not physically meaningful to have grid cells with centre points within the physical roughness

height. From a mathematical/numerical point of view however the reason for this requirement is less clear and it should actually be possible to have $y_P < k_{S,ground} = k_{S,ABL} \approx 30y_0$. This would solve to a large extent the problems of horizontal homogeneity reported in this paper. Note that this implies a code modification.

Instead of k_S-type wall functions, y_0-type wall functions can be used in which the roughness is expressed as a function of the aerodynamic roughness length y_0 instead of k_S. In this case, the requirements for CFD simulation of ABL flow relating to k_S are no longer applicable. For the standard k-ε turbulence model, an appropriate set of inlet profiles and y_0-type wall functions was provided by Richards and Hoxey (1993). These wall functions have a similar form as the ABL inlet profiles themselves: Eqs. (1-3) or Eqs. (2,5-6) and they provide horizontal homogeneity when the standard k-ε model constants satisfy Eq. (4) because then these equations form an analytical solution to this model. Unfortunately, in many existing CFD codes such wall functions are neither implemented nor can the user always implement them easily at present.

It is important to note that, strictly speaking, horizontal homogeneity can only be obtained if the inlet profiles of mean wind speed and turbulence properties are consistent with the turbulence model (including its constants) and with the wall functions and their roughness modification. This is the case for the combination of the inlet profiles in Eqs. (1-3) or Eqs. (2,5-6), the standard k-ε model with its constants satisfying Eq. (4) and wall functions based on the same equations as the inlet profiles. In other cases, horizontal homogeneity will not be obtained, e.g. when measured inlet profiles different from Eqs. (1-3) or Eqs. (2,5-6) are used. In this case a simulation in an empty domain, prior to the actual simulation with the building models present, is required to assess the extent of the horizontal inhomogeneity and its acceptability.

k_S-type and y_0-type wall functions are generally quite similar. Indeed, wall functions in Eqs. (1-3,5-6) and those in Eqs. (9,10,12,14-15) have a very similar or even identical shape and were matched earlier to find the k_S-value corresponding to a certain y_0. y_0-type wall functions are reported to perform very well in producing horizontally homogeneous ABL flow when y_P is much smaller than $k_{S,ABL} \approx 30y_0$ (Richards et al., 2002, Mochida et al., 2002, Bitsuamlak et al., 2006). This supports the idea that violating "$y_P > k_S$" should also be possible for k_S-type wall functions. However, due to current restrictions in several CFD codes including Fluent 6.2 and Ansys CFX 10.0, the requirement $y_P > k_S$ still has to be satisfied, and to limit horizontal inhomogeneity one has to resort to one or several of the remedial measures reported in Section 7.1.

8. Summary and conclusions

The accuracy of CFD simulations for atmospheric studies such as pollutant dispersion and deposition can be seriously compromised when wall-function roughness modifications based on experimental data for sand-grain roughened pipes and channels (k_S-type wall functions) are applied at the bottom of the computational domain. This type of roughness modification is currently present in many CFD codes including Fluent 6.2 and Ansys CFX 10.0. The problems typically manifest themselves as unintended changes (streamwise gradients) in the vertical mean wind speed and turbulence profiles as they travel through the computational domain (horizontal homogeneity problem). These gradients can – at least partly – be held responsible for the discrepancies sometimes found between seemingly identical CFD simulations performed with different CFD codes and between CFD simulations and measurements.

The problems are caused because it is generally impossible to simultaneously satisfy all four requirements for ABL flow simulations when k_S-type wall functions are used. The extent of the streamwise gradients depends on various simulation characteristics and settings, including the inlet profiles, the turbulence model, the type of wall functions, the near-wall grid resolution, the roughness height and the roughness constant.

The best solution to this problem is to alleviate the requirement $y_P > k_S$. This can be done either by using y_0-type wall functions or using k_S-type wall functions in CFD code formulations that allow violating this requirement. However, at the time of writing this paper, several CFD codes including Fluent 6.2 and Ansys CFX 10.0 allow neither of these options, in which case one or more of the remedial measures mentioned in Section 7.1 should be considered.

Irrespective of the type of simulation, the inlet profiles, turbulence model, wall functions and near-wall grid resolution used, it is advisable to always assess the extent of horizontal inhomogeneity by a simulation in an empty computational domain prior to the actual simulation with the obstacle models present. Sensitivity tests in an empty computational domain are of critical importance. In addition, for every CFD simulation it is advisable to always report not only the inlet profiles but also the incident flow profiles obtained from the simulation in the empty domain because they characterise the real flow to which the building models are subjected.

Acknowledgements

This research has been conducted while the first author was a post-doctoral research fellow of the FWO-Flanders (Research Fund – Flanders), an organization that supports and stimulates fundamental research in Flanders (Belgium). Their financial contribution is gratefully acknowledged. The authors also wish to express

their gratitude for the valuable discussions with Dr. Jörg Franke, Dr. Alan Huber, Dr. Bob Meroney, Dr. David Banks and Ir. David Dooms.

References

Ansys Ltd., 2005. Ansys CFX-solver, Release 10.0: Theory. Canonsburg.

Bitsuamlak, G.T., Stathopoulos, T., Bedard, C., 2004. Numerical evaluation of wind flow over complex terrain: Review. Journal of Aerospace Engineering 17 (4), 135-145. (doi:10.1061/(ASCE)0893-1321(2004)17:4(135))

Bitsuamlak, G., Stathopoulos, T., Bedard, C., 2006. Effects of upstream two-dimensional hills on design wind loads: A computational approach. Wind and Structures 9(1), 37-58.

Blocken, B., Carmeliet, J., 2002. Spatial and temporal distribution of driving rain on a low-rise building. Wind and Structures 5(5), 441-462.

Blocken, B., Roels, S., Carmeliet, J., 2004. Modification of pedestrian wind comfort in the Silvertop Tower passages by an automatic control system. Journal of Wind Engineering and Industrial Aerodynamics 92(10), 849-873. (doi:10.1016/j.jweia.2004.04.004)

Blocken, B., Carmeliet, J. 2004. A review of wind-driven rain research in building science. Journal of Wind Engineering and Industrial Aerodynamics 92(13), 1079-1130. (doi:10.1016/j.jweia.2004.06.003)

Blocken, B., Carmeliet, J. 2006. The influence of the wind-blocking effect by a building on its wind-driven rain exposure. Journal of Wind Engineering and Industrial Aerodynamics 94(2), 101-127. (doi:10.1016/j.jweia.2005.11.001)

Blocken, B., Carmeliet, J., Stathopoulos, T. 2006. CFD evaluation of the wind speed conditions in passages between buildings – effect of wall-function roughness modifications on the atmospheric boundary layer flow. Journal of Wind Engineering and Industrial Aerodynamics. Accepted for publication.

Castro, I.P., Robins, A.G. 1977. The flow around a surface mounted cube in a uniform and turbulent shear flow. Journal of Fluid Mechanics 79(2), 307-335.

Cebeci, T., Bradshaw, P., 1977. Momentum transfer in boundary layers. Hemisphere Publishing Corporation, New York.

Davenport, A.G., 1960. Rationale for determining design wind velocities, Journal of the Structural Division, Proceedings American Society Civil Engineers 86: 39-68.

Davenport A.G., 1961. The application of statistical concepts to the wind loading of structures, Proceedings Institution of Civil Engineers, August.

Durbin, P.A., Petterson Reif, B.A., 2001. Statistical theory and modelling for turbulent flows, John Wiley & Sons, Chichester.

Fluent Inc., 2005., Fluent 6.2 User's Guide, Fluent Inc., Lebanon.

Franke, J., Hirsch, C., Jensen, A.G., Krüs, H.W., Schatzmann, M., Westbury, P.S., Miles, S.D., Wisse, J.A., Wright, N.G., 2004. Recommendations on the use of CFD in wind engineering. Proceedings of the International Conference on Urban Wind Engineering and Building Aerodynamics, in: van Beeck JPAJ (Ed.), COST Action C14, Impact of Wind and Storm on City Life Built Environment, von Karman Institute, Sint-Genesius-Rode, Belgium, 5 - 7 May 2004.

Franke, J., Frank, W. 2005. Numerical simulation of the flow across an asymmetric street intersection, in: Náprstek, J., Fischer, C. (Eds.), Proceedings of the 4EACWE, 11-15 July 2005, Prague, Czech Republic.

Gao, Y., Chow, W.K., 2005. Numerical studies on air flow around a cube. Journal of Wind Engineering and Industrial Aerodynamics 93(3), 115-135.

Harris, R.I., Deaves, D.M., 1981. The structure of strong winds. Wind engineering in the eighties. Proc. of the CIRIA Conference, 12-13 November 1980, Construction Industry Research and Information Association, London, Paper 4.

Ioselevich, V.A., Pilipenko, V.I., 1974. Logarithmic velocity profile for flow of a weak polymer solution near a rough surface. Sov. Phys. Dokl. 18: 790.

Jones, W.P., Launder, B.E., 1972. The prediction of laminarization with a 2-equation model of turbulence. International Journal of Heat and Mass Transfer 15, 301.

Launder, B.E., Spalding, D.B., 1974. The numerical computation of turbulent flows, Computer Methods in Applied Mechanics and Engineering 3, 269-289.

Mathews, E.H., 1987. Prediction of the wind-generated pressure distribution around buildings. Journal of Wind Engineering and Industrial Aerodynamics 25, 219-228.

Meroney, R.N., 2004. Wind tunnel and numerical simulation of pollution dispersion: a hybrid approach. Working paper, Croucher Advanced Study Insitute on Wind Tunnel Modeling, Hong Kong University of Science and Technology, 6-10 December, 2004, 60 pp.

Miles, S., Westbury, P., 2003. Practical tools for wind engineering in the built environment. QNET-CFD Network Newsletter: 2, 2, pp. 11-14.

Mochida, A., Tominaga, Y., Murakami, S., Yoshie, R., Ishihara, T., Ooka, R., 2002. Comparison of various k-ε models and DSM applied to flow around a high-rise building – report on AIJ cooperative project for CFD prediction of wind environment. Wind and Structures 5(2-4), 227-244.

Moonen, P., Blocken, B., Roels, S., Carmeliet, J., 2006. Numerical modeling of the flow conditions in a closed-circuit low-speed wind tunnel. Journal of Wind Engineering and Industrial Aerodynamics. In press. (doi:10.1016/j.jweia.2006.02.001)

Nikuradse, J., 1933. Strömungsgesetze in rauhen Rohren. Forschg. Arb. Ing.-Wes. No. 361.

Quinn, A.D., Wilson, M., Reynolds, A.M., Couling, S.B., Hoxey, R.P., 2001. Modelling the dispersion of aerial pollutants from agricultural buildings – an evaluation of computational fluid dynamics (CFD). Computers and Electronics in Agriculture 30, 219-235.

Reichrath, S., Davies, T.W., 2002. Using CFD to model the internal climate of greenhouses: past, present and future. Agronomie 22 (1), 3-19.

Richards, P.J., 1989. Computational modelling of wind flows around low rise buildings using PHOENIX. Report for the ARFC Institute of Engineering Research Wrest Park, Silsoe Research Institute, Bedfordshire, UK.

Richards, P.J., Younis, B.A., 1990. Comments on "Prediction of the wind-generated pressure distribution around buildings" by E.H. Mathews. Journal of Wind Engineering and Industrial Aerodynamics 34, 107-110.

Richards, P.J., Hoxey, R.P., 1993. Appropriate boundary conditions for computational wind engineering models using the k-ε turbulence model. Journal of Wind Engineering and Industrial Aerodynamics 46&47, 145-153.

Richards, P.J., Quinn, A.D., Parker, S., 2002. A 6 m cube in an atmospheric boundary layer flow. Part 2. Computational solutions. Wind and Structures 5(2-4), 177-192.

Riddle, A., Carruthers, D., Sharpe, A., McHugh, C., Stocker, J., 2004. Comparisons between FLUENT and ADMS for atmospheric dispersion modelling. Atmospheric Environment 38(7), 1029-1038.

Schlichting, H., 1968. Boundary-layer theory. McGraw-Hill, 6th edition.

Stathopoulos, T., 1997. Computational wind engineering: Past achievements and future challenges. Journal of Wind Engineering and Industrial Aerodynamics 67-68, 509-532. (doi:10.1016/S0167-6105(97)00097-4)

White, F.M., 1991. Viscous fluid flow.McGraw-Hill, Second edition.

Wieringa, J., 1992. Updating the Davenport roughness classification. Journal of Wind Engineering and Industrial Aerodynamics 41-44, 357-368.

Zhang, C.X., 1994. Numerical prediction of turbulent recirculating flows with a k-ε model. Journal of Wind Engineering and Industrial Aerodynamics 51, 177-201.

Appendix A: List of symbols

B	integration constant in the log law
C_S	roughness constant
$C_{\varepsilon 1}$, $C_{\varepsilon 1}$, C_μ	constants in the k-ε model
e	inhomogeneity error (%)
E	empirical constant for a smooth wall in wall function (≈ 9.793)
k	turbulent kinetic energy (m²/s²)
k_S	equivalent sand-grain roughness height (m)
k_S^+	dimensionless equivalent sand-grain roughness height
L, H	length and height of computational domain (m)
P	centre point of wall-adjacent cell
TI	turbulence intensity
u_τ	wall-function friction velocity (m/s)
u^*	wall-function friction velocity (m/s)
u^*_{ABL}	ABL friction velocity (m/s)
u^+	dimensionless mean streamwise wind speed
U	mean streamwise wind speed (m/s)
x, y	streamwise and height co-ordinate (m)
y_0	aerodynamic roughness length (m)
y_P	distance from point P to the wall (m)
y^+	dimensionless wall unit
ε	turbulence dissipation rate (m²/s³)
κ	von Karman constant (0.4 ~ 0.42)
μ	dynamic molecular viscosity (kg/ms)
μ_t	dynamic turbulent viscosity (kg/ms)
ν	kinematic molecular viscosity (m²/s)
ρ	fluid density (kg/m³)
σ_ε	constant in the k-ε model

τ_w	wall shear stress (Pa)
φ	flow variable
ω	specific dissipation rate (1/s)
ΔB	roughness function
Δx	control volume length (m)

Figure captions

Fig. 1. Computational domain with building models for CFD simulation of ABL flow – definition of inlet flow, approach flow and incident flow and indication of different parts in the domain for roughness modelling.

Fig. 2. Law of the wall for smooth and sand-grain roughened surfaces with the dimensionless sand-grain roughness height k_S^+ as a parameter.

Fig.3. Graphical representation of fitting the mean-velocity ABL log-law inlet profile to the wall function for mean velocity in the centre point P of the wall-adjacent cell.

Fig. 4. CFD simulation results illustrating the streamwise gradients in the vertical profiles of (a) mean wind speed U; (b) turbulent kinetic energy k; (c) turbulence dissipation rate ε and (d) turbulence intensity TI at different downstream distances in the empty domain (x-coordinate). The left column shows the lowest 500 m of the boundary layer; the right column shows the lowest 50 m.

Fig. 5. CFD simulation results: relative changes (inhomogeneity errors) of the values of mean wind speed U, turbulent kinetic energy k, turbulence dissipation rate ε and turbulence intensity TI at two heights (y = 2 m and y = 20 m) and at various downstream positions in the empty domain (x-coordinate). All changes are expressed as positive percentage values relative to the values at the inlet of the domain (x = 0).

Fig. 6. Computational mesh with variable height of the wall-adjacent cells along the length of the domain.

Fig. 7. (a-b) Fine and coarse vertical near-ground mesh distribution at the inlet plane. (c-d) Corresponding mean wind speed and turbulence intensity profiles at the inlet of the domain: the analytical profile (imposed boundary condition) and the CFD profiles (one variable value per cell) for the fine and the coarse mesh distribution.

Fig. 8. CFD simulation results: relative changes (inhomogeneity errors) of the values of mean wind speed U and turbulence intensity TI at two heights (y = 2 m and y =20 m) and at various downstream positions in the empty domain (x-coordinate), for three options: NC = no correction, ALK = artificially lower turbulent kinetic energy, WSS = wall shear stress imposed at the bottom of the domain. All changes are expressed as positive percentage values relative to the values at the inlet of the domain (x = 0).

Fig. 9. CFD simulation results in terms of inlet (x = 0 m) and downstream (x = 10 000 m) vertical profiles of (a) streamwise wind speed U and (b) turbulence intensity TI for two cases: without correction and with wall shear stress imposed at the bottom of the empty domain.

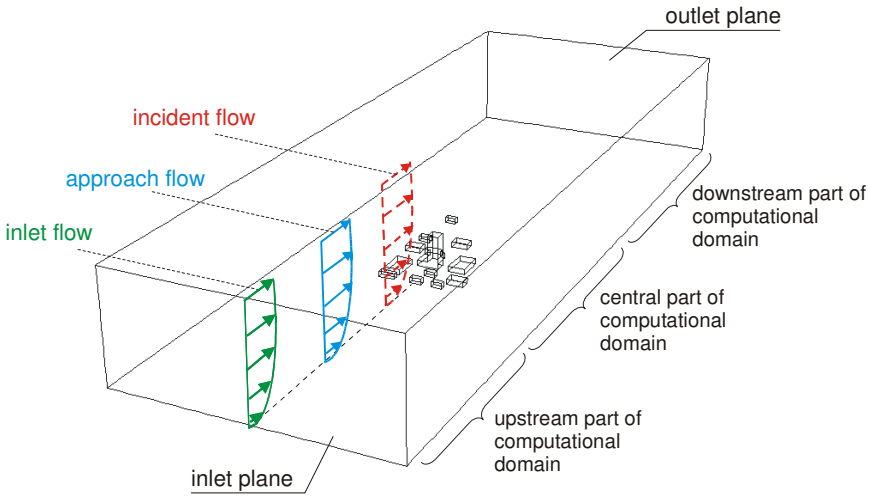

FIGURE 1

Fig. 1. Computational domain with building models for CFD simulation of ABL flow – definition of inlet flow, approach flow and incident flow and indication of different parts in the domain for roughness modelling.

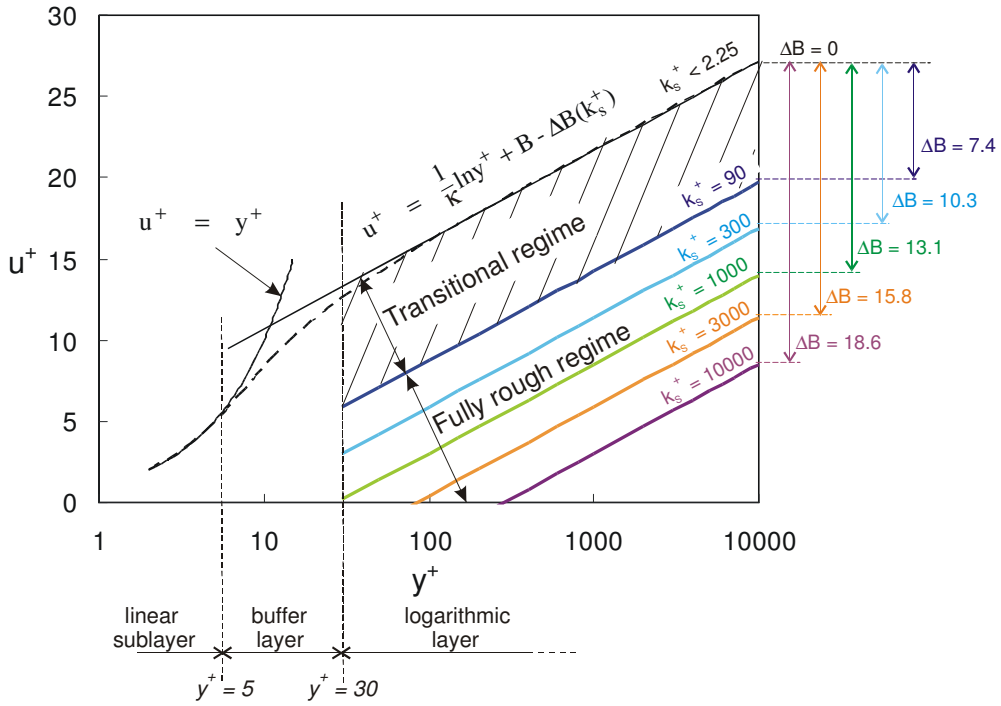

FIGURE 2

Fig. 2. Law of the wall for smooth and sand-grain roughened surfaces with the dimensionless sand-grain roughness height k_S^+ as a parameter.

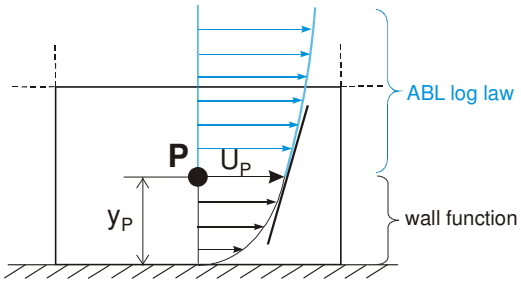

FIGURE 3

Fig.3. Graphical representation of fitting the mean-velocity ABL log-law inlet profile to the wall function for mean velocity in the centre point P of the wall-adjacent cell.

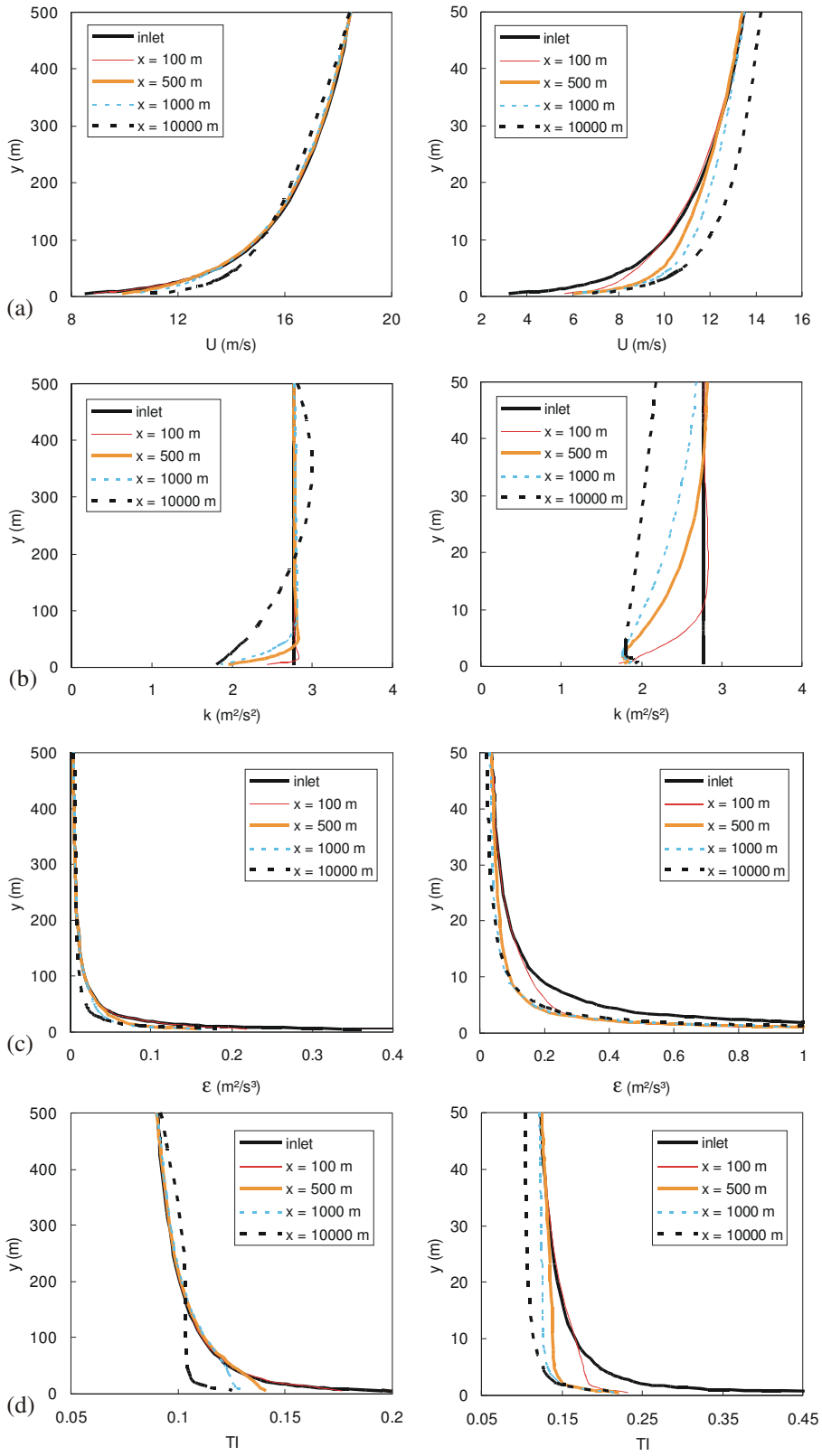

FIGURE 4

Fig. 4. CFD simulation results illustrating the streamwise gradients in the vertical profiles of (a) mean wind speed U; (b) turbulent kinetic energy k; (c) turbulence dissipation rate ε and (d) turbulence intensity TI at different downstream distances in the empty domain (x-coordinate). The left column shows the lowest 500 m of the boundary layer; the right column shows the lowest 50 m.

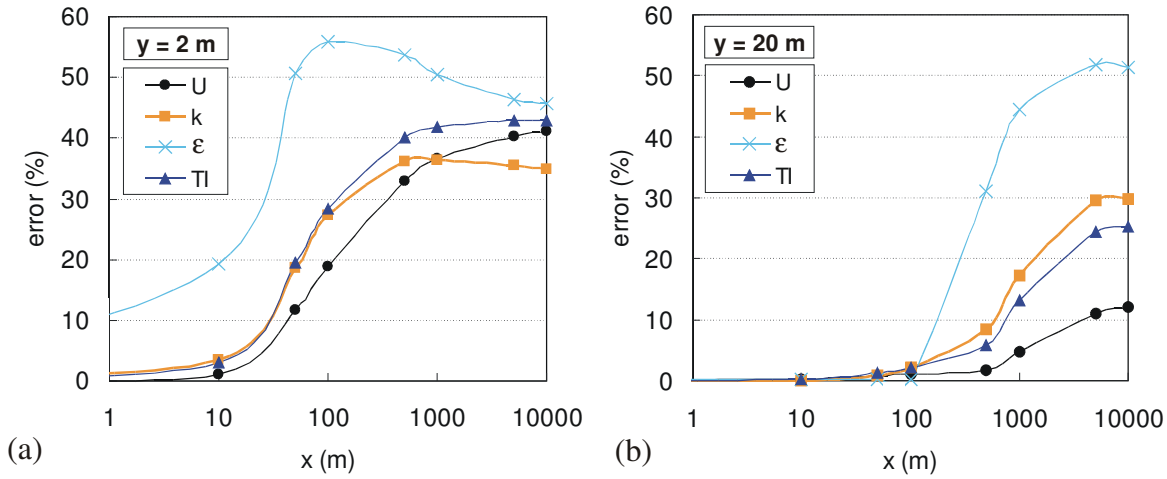

FIGURE 5

Fig. 5. CFD simulation results: relative changes (inhomogeneity errors) of the values of mean wind speed U, turbulent kinetic energy k, turbulence dissipation rate ε and turbulence intensity TI at two heights (y = 2 m and y = 20 m) and at various downstream positions in the empty domain (x-coordinate). All changes are expressed as positive percentage values relative to the values at the inlet of the domain (x = 0).

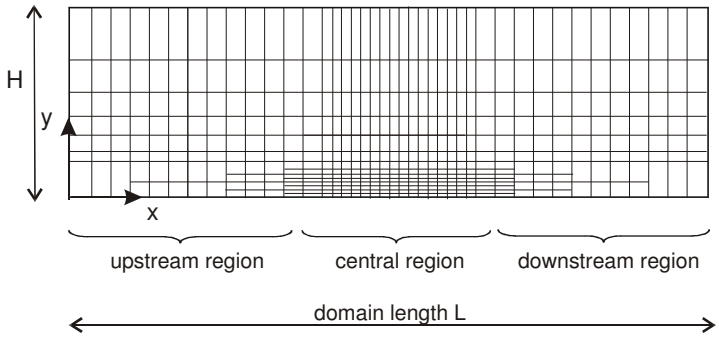

FIGURE 6

Fig. 6. Computational mesh with variable height of the wall-adjacent cells along the length of the domain.

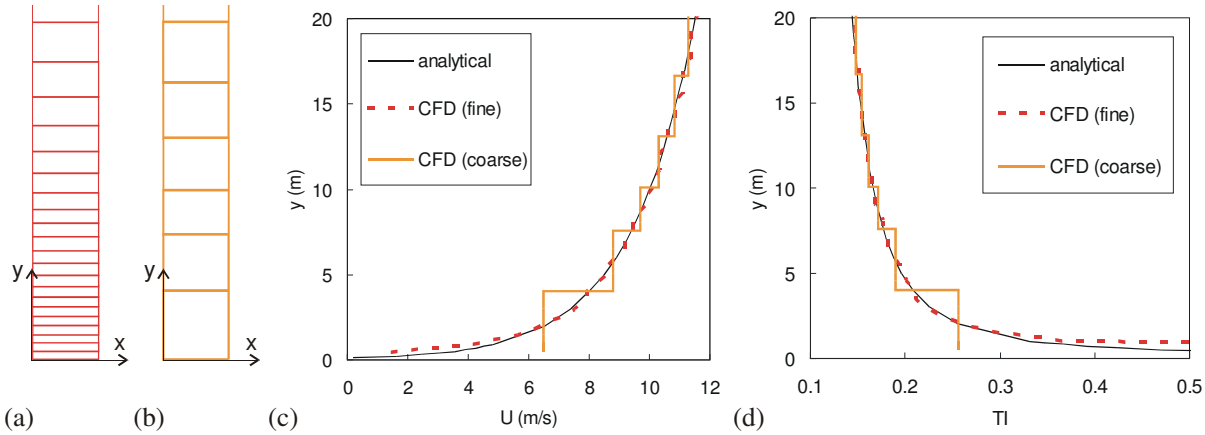

FIGURE 7

Fig. 7. (a-b) Fine and coarse vertical near-ground mesh distribution at the inlet plane. (c-d) Corresponding mean wind speed and turbulence intensity profiles at the inlet of the domain: the analytical profile (imposed boundary condition) and the CFD profiles (one variable value per cell) for the fine and the coarse mesh distribution.

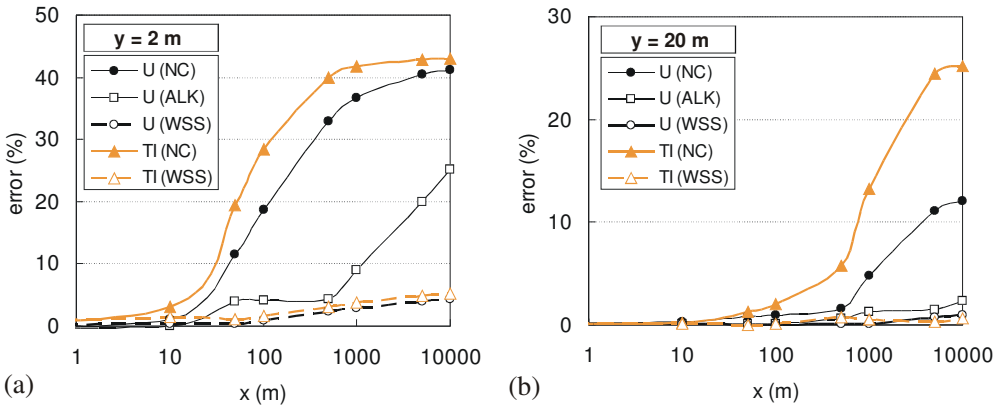

FIGURE 8

Fig. 8. CFD simulation results: relative changes (inhomogeneity errors) of the values of mean wind speed U and turbulence intensity TI at two heights (y = 2 m and y =20 m) and at various downstream positions in the empty domain (x-coordinate), for three options: NC = no correction, ALK = artificially lower turbulent kinetic energy, WSS = wall shear stress imposed at the bottom of the domain. All changes are expressed as positive percentage values relative to the values at the inlet of the domain (x = 0).

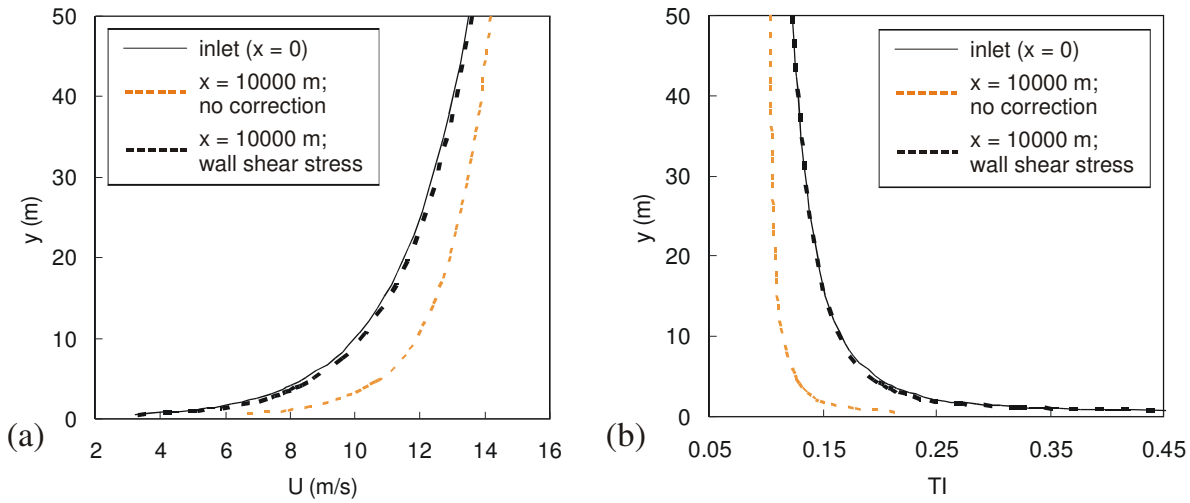

FIGURE 9

Fig. 9. CFD simulation results in terms of inlet (x = 0 m) and downstream (x = 10 000 m) vertical profiles of (a) streamwise wind speed U and (b) turbulence intensity TI for two cases: without correction and with wall shear stress imposed at the bottom of the empty domain.